



**Discover Generics**

Cost-Effective CT & MRI Contrast Agents

**FRESENIUS  
KABI**

**WATCH VIDEO**

**AJNR**

**4D-DSA for Assessment of the  
Angioarchitecture and Grading of Cranial  
Dural AVF**

P.F. Samp, F. Keil, R. du Mesnil, A. Birkhold, M.  
Kowarschik, E. Hattingen and J. Berkefeld

This information is current as  
of June 7, 2025.

*AJNR Am J Neuroradiol* published online 12 October 2023  
<http://www.ajnr.org/content/early/2023/10/12/ajnr.A8008>

# 4D-DSA for Assessment of the Angioarchitecture and Grading of Cranial Dural AVF

 P.F. Samp,  F. Keil,  R. du Mesnil,  A. Birkhold,  M. Kowarschik,  E. Hattingen, and  J. Berkefeld



## ABSTRACT

**BACKGROUND AND PURPOSE:** Time-resolved 3D rotational angiography (4D-DSA) has been used to demonstrate details of the angioarchitecture of AVM, whereas it has rarely been used to describe features of dural AVF. In this exploratory study, we analyzed dural AVFs with a novel 4D software prototype, developed and provided by Siemens, to determine whether identification of the location of the fistulous point, grading, and treatment planning were feasible.

**MATERIALS AND METHODS:** 4D-DSA volumes were calculated from existing 3D rotational angiography data sets of patients with dural AVFs. The 4D-DSA volumes were displayed in a virtual DSA mode and MPR or MIP in 3 orthogonal planes and compared with 2D-DSA by 2 experienced neuroradiologists. Fusions with unenhanced CT or MR images were used to improve visualization of adjacent anatomic structures.

**RESULTS:** Comparison with 2D-DSA showed that evaluation of the fistulous point and grading according to the classification of Borden, Cognard, or Barrow was feasible in 26 of 27 cases. In 8 of 27 cases, 4D-DSA was considered advantageous for determining the fistulous point and the course of the draining vein in the dural AVF with cortical venous drainage, especially in the frontoethmoidal and frontoparietal regions. In 6 cases, the display of angioarchitecture was considered inferior to that of 2D-DSA due to motion artifacts, suboptimal selection of the injected vessel, and lack of temporal resolution.

**CONCLUSIONS:** Detailed analysis of dural AVFs according to the standardized display of 4D-DSA volumes was feasible and helpful in understanding the angioarchitecture in selected cases. Further improvement and validation of the 4D software should solidify the complementary role of 4D-DSA to conventional 2D-DSA series.

**ABBREVIATIONS:** DAVF = dural AVF; 3DRA = 3D rotational angiography; 4D-DSA = time-resolved 3D rotational angiography; ECA = external carotid artery; fpCBCTA = flat panel conebeam CTA

2D-DSA remains the standard for diagnosis, grading, and treatment planning of patients with dural AVFs (DAVFs). Although noninvasive imaging techniques such as MRA and CTA have improved in this regard,<sup>1-3</sup> their spatial and temporal resolution is still inferior to that of angiographic imaging with modern flat panel DSA equipment. 3D rotational angiography (3DRA) is frequently used in addition to DSA projection images for optimal visualization of the shunt zone in any projection or through the generation of flat panel conebeam CTA (fpCBCTA) cross-sectional images.<sup>4</sup>

It has been demonstrated that time-resolved 3D rotational angiography (4D-DSA) with its combination of high spatial and temporal resolution could be favorable for detailed analysis of the microvasculature of the shunt zone of an AVM.<sup>4-9</sup> Previous studies have included only a limited number of DAVF cases.<sup>4,6,10</sup> Furthermore, 4D-DSA volumes and 4D-fpCBCTA reconstructions were not systematically evaluated for identifying the fistulous point and grading or planning of endovascular or surgical treatment of DAVF.

Within this exploratory study, we used a novel software prototype, developed and provided by Siemens, to calculate 4D-DSA from existing 3DRA data sets. By comparing 4D-DSA in a standardized display with virtual DSA and cross-sectional images with 2D-DSA, we aimed to obtain a first impression of the potential diagnostic value for pretherapeutic assessment of patients with DAVFs.


## MATERIALS AND METHODS

We reviewed the records of patients with cranial DAVFs between 2016 and 2021. We included all cases of DAVFs that had DSA

Received June 5, 2023; accepted after revision August 30.

From the Institute of Neuroradiology (P.F.S., F.K., R.d.M., E.H., J.B.), University Hospital Frankfurt, Goethe University Frankfurt, Frankfurt am Main, Germany; and Siemens Healthcare (A.B., M.K.), Forchheim, Germany.

Please address correspondence to Patrick F. Samp, MD, Institute of Neuroradiology, University Hospital Frankfurt, Goethe University Frankfurt, Schleusenweg 2-16, 60528 Frankfurt am Main, Germany; e-mail: patrickfelix.samp@kgu.de

 Indicates open access to non-subscribers at [www.ajnr.org](http://www.ajnr.org)

 Indicates article with online supplemental data.

<http://dx.doi.org/10.3174/ajnr.A8008>

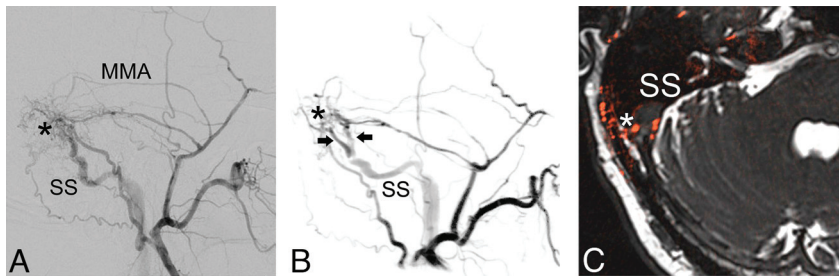


**FIG 1.** A DAVF between the middle meningeal artery (MMA), occipital artery and venous channels in the wall of the right lateral sinus with postthrombotic changes. Comparison of a standard lateral projection in 2D-DSA (A) and a slightly modified oblique projection of a virtual DSA-reconstruction (B) as well as an axial fusion image (C) derived from a 4D-DSA data set fused with a CISS MR imaging sequence. The possibility to choose an optimized projection on 4D-DSA improves the visualization of the arterial network at the fistulous point (asterisk) with connections to 2 venous channels (arrows) with Y-shaped convergence to a single venous channel in the wall of the sigmoid sinus (SS) with postthrombotic changes.

and 3DRA for treatment planning, being part of our routine protocol. We excluded patients without 3DRA. Our local ethics committee approved the study protocol. No additional patient consent was required.

2D-DSA series and 3DRA were obtained on a modified Axiom Artis zee biplane angiography system (Siemens) using an acquisition with a 260° rotation angle and a scan duration of 12 seconds. More recently, we used a new Artis icono biplane system (Siemens) with the same scan parameters. The interventionalist selected the DAVF-supplying artery from which 3DRA was performed. For the external carotid artery (ECA), 20 mL of nonionic contrast, iopromide (Ultravist 300; Bayer HealthCare), was injected by hand to reduce patient movement due to irritating heat sensations in the viscerocranium. For the ICA or the vertebral artery, we used an automatic injector with a flow rate of 3 mL/s.

4D-DSA volumes and 4D-fpCBCTA cross-sectional images were calculated from the 3DRA data sets on a dedicated research workstation (syngo X Workplace VD20; Siemens). A novel software prototype with an improved algorithm for 4D-DSA reconstructions, developed and provided by Siemens, was used. Compared with the commercially available syngo Dyna4D product (Siemens), the 4D-DSA software prototype adds a streak artifact removal method during the reconstruction of the initial 3D-DSA image. This is intended to reduce image-quality issues of 4D-DSA based on inconsistent 2D projection data due to noise and contrast agent dynamics. Multiplicative back-projection of 2D projection images into a static 3D image can lead to implausible vessel enhancement because contrast information from overlapping vessel segments cannot be entirely separated. Therefore, a physically motivated, plausibility-based flow constraint is applied to the 4D reconstruction process to prevent the appearance of incorrect or nonphysiologic vessel filling. This temporal artifact-reduction method takes into account that a particular vessel segment can be contrast-enhanced only under certain conditions. A recent study demonstrated these advantages when using the software prototype for an AVM compared with the commercially available syngo Dyna4D product.<sup>11</sup>

In our study, the 4D volumes were presented in a virtual DSA mode to allow direct comparison with conventional 2D-DSA

(Figs 1 and 2). For visualization of arterial feeders, the fistulous point, and draining veins, we selected the time point with the best filling of the DAVF and a projection with minimal overlay from adjacent vessels. 4D-fpCBCTA images were displayed in 3 orthogonal planes with variable section thickness between 1 and 10 mm, either as MPR or MIP, as well as Volume Rendering Technique (VRT). 2D-DSA was acquired at variable frame rates up to 6 frames/s in posteroanterior and lateral projections and, in selected cases, in additional oblique projections.

4D-DSA in a virtual DSA mode and 2D-DSA were rated by 2 independent reviewers. Furthermore, the added

value of 4D-fpCBCTA reconstructions and fusions between unenhanced fpCBCTA and MR images was assessed.

The rating was performed on a scale of 0 to 4:

- 0 = Not evaluable (no grading possible)
- 1 = Poor (grading uncertain, limited image quality)
- 2 = Acceptable (grading possible, limited quality in several features)
- 3 = Good (grading possible, limited quality in a single feature)
- 4 = Very good (grading possible, high quality in all features).

The criteria for the analysis were the following:

- 1) Detection of arterial feeders
- 2) Location of the fistulous point or fistulous zone
- 3) Course and direction of flow in the draining sinus or vein
- 4) Grading of the fistula according to the classifications of Cognard and Borden, as well as Barrow in the case of carotid cavernous fistula
- 5) Suitability of arterial or venous vessels as access for endovascular therapy
- 6) Anatomic neighborhood of the arteriovenous shunt.

The results were summarized in a table, and we illustrated the main features of 4D in a case series. We calculated the interrater agreement using a linearly weighted Cohen  $\kappa$  coefficient within SPSS, Version 29.0 (IBM).

## RESULTS

We included data sets from 27 DAVFs in 26 patients, 21 men and 5 women. Table 1 shows the patient and DAVF characteristics.

The largest group ( $n = 9$ , 33%) had DAVFs located at the distal transverse sinus, in whom pulsatile tinnitus was the most frequent clinical symptom. A small number of cases ( $n = 5$ , 18%) presented with intracranial hemorrhage. Focal neurologic deficits occurred in 5 cases. Twenty-six percent of cases ( $n = 7$ ) had low-grade DAVFs (Borden I, Cognard I and IIa), 63% ( $n = 17$ ) had high-grade DAVFs (Borden II and III, Cognard IIb, III, and IV), and 11% ( $n = 3$ ) had symptomatic carotid cavernous fistulas (Barrow A and D), with ocular symptoms such as chemosis and proptosis, as well as various cranial nerve deficits.

**Table 1: Patient overview with DAVF grading according to Cognard or Barrow**

Age (yr)	Sex	Location	Type	Symptoms	Therapy
62	Male	Frontoethmoidal	III	None	Transvenous coiling
64	Male	Frontoethmoidal	IV	None	Transvenous coiling
72	Male	Frontoethmoidal	IV	None	Transvenous coiling
51	Female	Frontoethmoidal	IV	None	Surgery
48	Male	Frontal	IV	Headache, vertigo	Transarterial Onyx
43	Male	Frontal	III	None	Transarterial Onyx
45	Male	Frontal	III	Visual field loss	Transarterial Onyx
66	Male	Frontal	III	Acute cerebral hemorrhage	Surgery
69	Male	Infratentorial	III	None	Transarterial Onyx
54	Male	Infratentorial	III	Acute cerebral hemorrhage	Surgery
57	Male	Infratentorial	IV	Acute cerebral hemorrhage	Surgery
75	Female	Occipital	IIa	Pulsatile tinnitus	Transarterial Onyx
47	Male	Occipital	I	Pulsatile tinnitus	Transarterial Onyx
77	Male	Occipital	IIa	Pulsatile tinnitus	Transarterial Onyx
79	Male	Occipital	IV	Acute cerebral hemorrhage	Transarterial Onyx
72	Male	Occipital	I	Pulsatile tinnitus	None
64	Male	Occipital	IIa	Pulsatile tinnitus	Transarterial Onyx
70	Male	Occipital	I	Pulsatile tinnitus	Transvenous coiling
84	Female	Occipital	IIb	Pulsatile tinnitus	None
59	Male	Occipital	I	Pulsatile tinnitus	None
31	Male	Temporo-occipital	III	Acute cerebral hemorrhage	Transarterial Onyx
31	Male	Temporo-occipital	III	None	Surgery
62	Male	Tentorial	IV	Headache	Transarterial Onyx
53	Male	Tentorial	IV	Hemiparesis	Radisurgery
62	Male	Carotid cavernous	A	Cranial nerve deficit (II)	Transarterial coiling
68	Female	Carotid cavernous	A	Cranial nerve deficit (III+IV)	Transarterial coiling
67	Female	Carotid cavernous	D	Cranial nerve deficit (IV)	Transvenous coiling

**Table 2: Advantages and disadvantages of 4D-DSA compared with 2D-DSA**

	No.	%
4D considered equal to 2D	13	48.1
4D considered advantageous to 2D	8	29.7
Improved projection	6	22.2
Reduction of vessel overlay	4	14.8
Display of adjacent anatomic structures	4	14.8
4D considered inferior to 2D	6	22.2
Incorrect grading	2	7.4
Endovascular access not displayed	2	7.4
Contrast injection too early	1	3.7
Incomplete display of arterial feeders	4	18.5
Pseudoretrograde display of small vessels	2	7.4
Motion artifacts	4	14.8

All patients with intracranial hemorrhage and neurologic deficits presented with higher DAVF grades with drainage via the cortical veins, or carotid cavernous fistulas with drainage via orbital veins.

Most patients ( $n = 24$ , 89%) received treatment after angiography. Only 3 cases remained untreated. Endovascular treatment was the preferred treatment option with either transarterial embolization with Onyx ( $n = 11$ ; Covidien) or transvenous embolization with detachable coils ( $n = 5$ ). Neurosurgical treatment was performed in 5 patients with fistulas inaccessible to superselective catheterization. A single patient with a recurrent cortical DAVF was treated with radiosurgery after declining surgery.

The diagnosis of a DAVF and identification of the fistulous point based on 4D-DSA were feasible in 26 of 27 cases. Grading according to the classifications of Cognard or Barrow was identical to that of 2D-DSA in 25 of 27 cases. The rating of the image

quality for grading by 2 independent reviewers resulted in a linearly weighted Cohen  $\kappa$  coefficient of 0.653, indicating adequate and significant interrater agreement ( $P < .001$ ).

In terms of visualization quality, 4D-DSA was comparable with 2D-DSA in 21 of 27 cases. In 6 of 27 cases, 4D-DSA was considered inferior to 2D-DSA due to a combination of factors: incomplete filling of small arterial feeders ( $n = 4$ ), incorrect or “pseudoretrograde” visualization of flow direction in feeding arteries or draining veins ( $n = 2$ ), image degradation due to motion artifacts ( $n = 4$ ), or missing visualization of potential access for endovascular treatment ( $n = 2$ ). This issue resulted in incorrect grading in 2 cases, one primarily due to motion artifacts and the other due to missing visualization of retrograde flow in the transverse sinus, therefore leading to incorrect grading of a Cognard IIa DAVF as Cognard I.

However, in 8 of 27 data sets, analysis of virtual DSA and 4D-fpCBCTA provided additional information regarding the exact location of the fistulous point and the course of the initial segment of the draining vein as targets for treatment. The main advantages (Table 2) in these 8 cases were improved visualization of the arteriovenous transition due to free selection of an optimal projection ( $n = 6$ ), less overlay of veins due to selection of an optimal time point of the 4D-DSA ( $n = 4$ ), and the possibility of displaying the adjacent anatomic structures ( $n = 4$ ). These advantages were especially found in high-grade DAVFs with cortical venous drainage (Fig 2), most notably in the frontoethmoidal and frontoparietal regions.

## DISCUSSION

The use of 4D-DSA volumes and 4D-fpCBCTA reconstructions for detailed analysis of the angioarchitecture and grading of cranial DAVFs was feasible and mostly comparable with 2D-DSA.



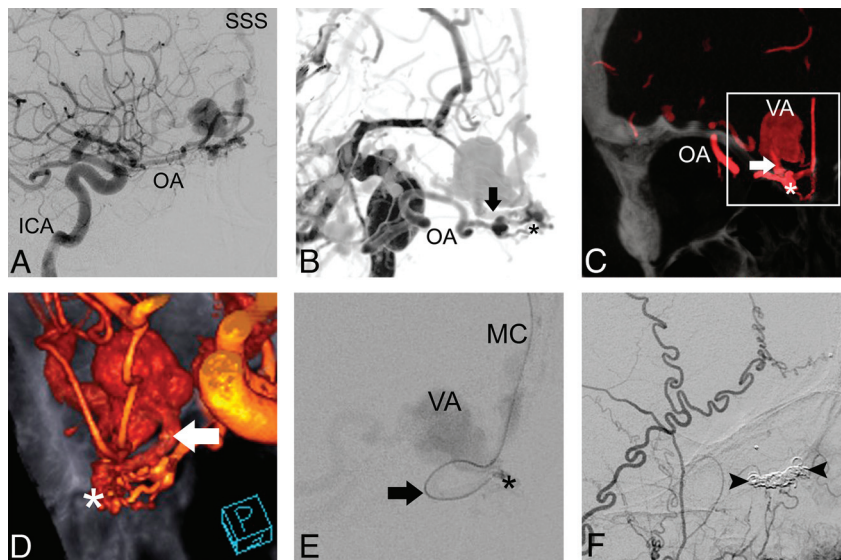


**FIG 2.** Comparison of a lateral standard projection in 2D-DSA (A) with an oblique projection in virtual DSA derived from 4D-DSA (B) and 4D-DSA coronal CT MIP (C) and volume rendering with an overlay of skull in an oblique zoomed-in projection (D). The 2D-DSA standard projection shows the frontoethmoidal DAVF supplied by the ophthalmic artery (OA) with drainage into the cortical veins and then the superior sagittal sinus (SSS). 4D-DSA images offer better visualization of the frontoethmoidal fistulous point (asterisk) and its anatomic relation to the draining vein (arrow), which is obscured in the standard projection of 2D-DSA, and the following venous aneurysm (VA). Note that the fistulous point is located within the olfactory groove. For endovascular therapy, a transvenous approach is selected with superselective positioning of the microcatheter (MC) in the draining vein past the VA (E), close to the fistulous point. After coiling (arrowheads) of the draining vein (F), we achieved complete embolization of the DAVF, as seen in the control angiogram of the ECA.

Correct grading, according to the classifications of Cognard or Barrow, was possible, except in 2 cases.

In selected cases, the new 4D method was considered advantageous in identifying the fistulous point and the initial segment of the draining vein as the main targets for treatment. The ability to visualize the shunt zone in any projection and at any time point of the scan was especially advantageous in cases with drainage into cortical veins or venous channels in the wall of a sinus. This ability may influence the decision as to whether the initial segment of the draining vein is suitable for transarterial penetration of Onyx without balloon protection of the adjacent sinus or for transvenous placement of coils. The 4D data may also be valuable for the planning of surgical or radiosurgical treatment. Fusion images with unenhanced fpCBCTA or MR images were used to demonstrate the relationship between the fistulous point and adjacent anatomic structures.

The question remains as to whether 4D is superior to 3DRA reconstructions without temporal resolution. In most cases, 3DRA may provide the same information. However, in cases with rapid flow or massive overlay by enlarged draining veins, the selection of a time point with the best visualization of the arteriovenous transition was helpful.

The main disadvantage of 4D-DSA was the limited suitability for planning of transarterial embolization with Onyx. In cases with multiple arterial feeders, the visualization of small-caliber meningeal arteries as the preferred access for the microcatheter was often incomplete or inferior to the superior spatial resolution of 2D DSA. Overlapping angiographic

phases continue to pose a relevant obstacle, requiring further improvement of the software prototype to enhance the validity of subsequent filling of small tortuous vessels.

We used a comparatively lengthy contrast bolus and scan duration to achieve sufficient filling of small vessels. Hand injection in ECA angiograms could also contribute to inconsistent vessel filling and bolus timing. We used hand injections to adapt the contrast volume and flow to the flow in the ECA branches and to minimize patient movement due to heat sensations associated with ECA contrast injection. Further systematic studies with different injection and scan protocols and use of an automatic injector may be necessary to optimize the filling of vessels with varying caliber and flow.

3DRA was acquired with an injection in only 1 feeding artery, whereas most DAVFs had several feeding arteries from multiple vascular territories. The interventionalist's selection was not always optimal for treatment planning. The accessibility of arteries and veins for superselective catheterization, especially as potential therapeutic

endovascular access, was not always considered during the diagnostic angiography.

We avoided repeat 3DRA acquisitions from different feeders for radiation protection. The modification of the scan angle (260° for 4D-DSA compared with 200° for standard 3D-DSA) and longer scan duration (12 seconds compared with 5 seconds) led to an increase in the radiation dose, which was still within reported doses for standard 3DRA and significantly less compared with 4D-CTA.<sup>12,13</sup> Future studies will use protocols with a reduction of the scan duration to 6 seconds, which should significantly decrease the radiation dose.

A complete display of all feeding arteries can be obtained through noninvasive CTA or MRA.

The main advantage of DSA and especially fpCBCTA is the unique spatial resolution, which greatly improves the visualization of the angioarchitecture compared with CTA or contrast-enhanced MRA.<sup>14</sup> The spatial and temporal resolution of 4D-DSA is notably superior to that of current time-resolved contrast-enhanced MRA, which was deemed insufficient for the grading of DAVFs.<sup>15</sup> In the future, new, time-resolved CTA and MRA techniques may further increase the value of the noninvasive imaging of DAVF.<sup>2,12,16,17</sup>

An important limitation of our study is its retrospective design with a small number of cases in a single center. Further multicenter studies are necessary to evaluate the usefulness and validity of 4D-DSA and 4D-fpCBCTA.

The interrater agreement was adequate considering the complexity of evaluating 4D-DSA and 4D-fpCBCTA. In our opinion,

the differences in ratings were minor and limited to the assessment of image quality. There were no major differences in rater opinions in terms of whether grading or identification of the fistulous point was possible.

We aimed to standardize the reconstruction parameters to improve postprocessing efficiency. Due to numerous manual steps, the average time for postprocessing was approximately 45 minutes. However, automated display of predefined reconstructions with optimal vessel contrast and window settings could substantially improve postprocessing, particularly for independent reviewers.

## CONCLUSIONS

Detailed analysis of the angioarchitecture of DAVFs with 4D-DSA volumes and fpCBCTA images is feasible and helpful for treatment planning in selected cases. At the current stage of development, 4D-DSA should be considered as complementary to 2D-DSA, and not as a substitute. Further validation of the method requires improvement of examination protocols and the 4D software.

**Disclosure forms** provided by the authors are available with the full text and PDF of this article at [www.ajnr.org](http://www.ajnr.org).

## REFERENCES

1. Ye X, Wang H, Huang Q, et al. **Four-dimensional computed tomography angiography is valuable in intracranial dural arteriovenous fistula diagnosis and fistula evaluation.** *Acta Neurol Belg* 2015;115:303–09 [CrossRef Medline](#)
2. In 't Veld M, Fronczek R, Dos Santos MP, et al. **High sensitivity and specificity of 4D-CTA in the detection of cranial arteriovenous shunts.** *Eur Radiol* 2019;29:5961–70 [CrossRef Medline](#)
3. Nishimura S, Hirai T, Sasao A, et al. **Evaluation of dural arteriovenous fistulas with 4D contrast-enhanced MR angiography at 3T.** *AJNR Am J Neuroradiol* 2010;31:80–85 [CrossRef Medline](#)
4. Lescher S, Gehrisch S, Klein S, et al. **Time-resolved 3D rotational angiography: display of detailed neurovascular anatomy in patients with intracranial vascular malformations.** *J Neurointerv Surg* 2017;9:887–94 [CrossRef Medline](#)
5. Keil F, Bergkemper A, Birkhold A, et al. **4D flat panel conebeam CTA for analysis of the angioarchitecture of cerebral AVMs with a novel software prototype.** *AJNR Am J Neuroradiol* 2022;43:102–09 [CrossRef Medline](#)
6. Lang S, Göllitz P, Struffert T, et al. **4D DSA for dynamic visualization of cerebral vasculature: a single-center experience in 26 cases.** *AJNR Am J Neuroradiol* 2017;38:1169–76 [CrossRef Medline](#)
7. Sandoval-Garcia C, Royalty K, Yang P, et al. **4D DSA a new technique for arteriovenous malformation evaluation: a feasibility study.** *J Neurointerv Surg* 2016;8:300–04 [CrossRef Medline](#)
8. Ognard J, Magro E, Caroff J, et al. **A new time-resolved 3D angiographic technique (4D DSA): description, and assessment of its reliability in Spetzler-Martin grading of cerebral arteriovenous malformations.** *J Neuroradiol* 2018;45:177–85 [CrossRef Medline](#)
9. Chen KK, Guo WY, Yang HC, et al. **Application of time-resolved 3D digital subtraction angiography to plan cerebral arteriovenous malformation radiosurgery.** *AJNR Am J Neuroradiol* 2017;38:740–46 [CrossRef Medline](#)
10. Srinivasan VM, Chintalapani G, Duckworth EA, et al. **Application of 4-dimensional digital subtraction angiography for dural arteriovenous fistulas.** *World Neurosurg* 2016;96:24–30 [CrossRef Medline](#)
11. Xiang W, Yan L, Zhao Y, et al. **Four-dimensional digital subtraction angiography to assess cerebral arteriovenous malformations.** *J Neuroimaging* 2023;33:67–72 [CrossRef Medline](#)
12. Radon MR, Chandran A, Bhojak M, et al. **Radiation dose reduction in 4D cerebral CT angiography by individualized estimation of cerebral circulation time.** *AJNR Am J Neuroradiol* 2016;37:2189–94 [CrossRef Medline](#)
13. Huizinga N, Keil F, Birkhold A, et al. **4D flat panel conebeam CTA for in vivo imaging of the microvasculature of the human cortex with a novel software prototype.** *AJNR Am J Neuroradiol* 2020;41:976–79 [CrossRef Medline](#)
14. Davis B, Royalty K, Kowarschik M, et al. **4D digital subtraction angiography: implementation and demonstration of feasibility.** *AJNR Am J Neuroradiol* 2013;34:1914–21 [CrossRef Medline](#)
15. Dissaux B, Eugène F, Ognard J, et al. **Assessment of 4D MR angiography at 3T compared with DSA for the follow-up of embolized brain dural arteriovenous fistula: a dual-center study.** *AJNR Am J Neuroradiol* 2021;42:340–46 [CrossRef Medline](#)
16. Balasubramanian AP, Kannath SK, Rajan JE, et al. **Utility of silent magnetic resonance angiography in the evaluation and characterisation of intracranial dural arteriovenous fistula.** *Clin Radiol* 2021;76:712.e1–e8 [CrossRef Medline](#)
17. Denby CE, Chatterjee K, Pullicino R, et al. **Is four-dimensional CT angiography as effective as digital subtraction angiography in the detection of the underlying causes of intracerebral haemorrhage: a systematic review.** *Neuroradiology* 2020;62:273–81 [CrossRef Medline](#)